NeuroImage: Clinical 22 (2019) 101702

Contents lists available at ScienceDirect

NeuroImage: Clinical

journal homepage: www.elsevier.com/locate/ynicl

Structural connectome alterations in patients with disorders of consciousness revealed by 7-tesla magnetic resonance imaging

Xufei Tan[a], Zhen Zhou[b,g], Jian Gao[c], Fanxia Meng[a], Yamei Yu[a], Jie Zhang[d], Fangping He[a], Ruili Wei[a], Junyang Wang[a], Guoping Peng[a], Xiaotong Zhang[e,f], Gang Pan[b,g,*], Benyan Luo[a,h,**]

[a] Department of Neurology, Brain Medical Centre, the First Affiliated Hospital, School of Medicine, Zhejiang University, Hangzhou, China
[b] State Key Lab of CAD&CG, Zhejiang University, Hangzhou, China
[c] Department of Rehabilitation, Hangzhou Hospital of Zhejiang CAPR, Hangzhou, China
[d] Department of Rehabilitation Medicine, Zhejiang Provincial People's Hospital, People's Hospital of Hangzhou Medical College, Hangzhou, China
[e] Interdisciplinary Institute of Neuroscience and Technology, Qiushi Academy for Advanced Studies, Zhejiang University, Hangzhou, China
[f] Center for Brain Imaging Science and Technology, College of Biomedical Engineering and Instrumental Science, Zhejiang University, Hangzhou, China
[g] College of Computer Science and Technology, Zhejiang University, Hangzhou, China
[h] School of Medicine, Zhejiang University, Collaborative Innovation Center for Brain Science, Hangzhou, China

ARTICLE INFO

Keywords:
Disorders of consciousness
Ultra-high field (7 T)
White matter
Diffusion MRI
Connectome
Transitivity

ABSTRACT

Although the functional connectivity of patients with disorders of consciousness (DOC) has been widely examined, less is known about brain white matter connectivity. The aim of this study was to explore structural network alterations for the diagnosis and prognosis of patients with chronic DOC. Eleven DOC patients and 11 sex- and age-matched controls were included in the study. Participants underwent diffusion magnetic resonance imaging (MRI) and T1-weighted structural MRI at 7 tesla (7 T). Graph-theoretical analysis and network-based statistics were used to analyze the group differences. Two patients were scanned twice for a longitudinal study to examine the relationship between connectome metrics and the patients' prognoses. Compared with healthy controls, DOC patients showed significantly elevated transitivity ($p < .001$), local efficiency ($p = .009$), and clustering coefficient ($p = .039$). When comparing the connectome metrics within the three groups (healthy controls, minimally conscious state (MCS), and vegetative state/unresponsive wakefulness syndrome (VS/UWS)), significant group differences were observed in transitivity ($p < .001$) and local efficiency ($p = .031$). Significantly increased transitivity was observed in vegetative state/unresponsive wakefulness syndrome compared with minimally conscious state ($p = .0217$, Bonferroni corrected). Transitivity showed significant negative correlations with the Coma Recovery Scale-Revised score ($r = -0.6902$, $p = .023$), consistent with the longitudinal study results. A subnetwork with significantly decreased structural connections was identified using network-based statistical analysis comparing DOC patients with healthy controls, which was mainly located in the frontal cortex, limbic system, and occipital and parietal lobes. This preliminary study suggests that graph theoretical approaches for assessing white matter connectivity may enable various states of DOC to be distinguished. Of the metrics analyzed, transitivity had a critical role in distinguishing the diagnostic groups. Larger cohorts will be necessary to confirm the predictive value of 7 T MRI in the prognosis of DOC patients.

1. Introduction

To study severe brain damage like disorders of consciousness (DOC), including vegetative state/unresponsive wakefulness syndrome (VS/UWS) (Laureys et al., 2010) and minimally conscious state (MCS) (Giacino et al., 2002), it is critical to understand changes in brain connectivity networks (Smith et al., 2009; Mayer et al., 2011; Shumskaya et al., 2012; Pandit et al., 2013; Sharp et al., 2014). DOC are caused by disruption of neural networks that constitute consciousness and its two essential components, arousal and awareness (Bodien et al., 2017). Recent advances in neuroimaging techniques have enabled the investigation of network connectivity in patients with DOC. Functional

* Correspondence to: G. Pan, College of Computer Science and Technology, Zhejiang University, Hangzhou, China.
** Correspondence to: B. Luo, Department of Neurology, Brain Medical Centre, the First Affiliated Hospital, School of Medicine, Zhejiang University, Hangzhou, China.
E-mail addresses: gpan@zju.edu.cn (G. Pan), luobenyan@zju.edu.cn (B. Luo).

https://doi.org/10.1016/j.nicl.2019.101702
Received 3 September 2018; Received in revised form 25 January 2019; Accepted 28 January 2019
Available online 29 January 2019

magnetic resonance imaging (fMRI) has become a common tool to investigate functional connectivity, which is a statistical measure of correlation between neuronal activities (Zhou et al., 2018). A growing number of studies have reported reduced functional connectivity in the default mode network (DMN) (Boly et al., 2009), fronto-parietal network (Long et al., 2016), and thalamo-cortical network (Crone et al., 2014) in patients with DOC.

Recently, white matter (WM) has drawn increasing attention among studies of DOC. The "disconnection hypothesis" has been proposed, which postulates that WM microstructure lesions result in the interruption of communication between cortical regions, thereby resulting in poorer cognitive performance (Cremers et al., 2016; Nazeri et al., 2015). Indeed, WM damage is an important determinant of cognitive impairment after brain injury. Studies on both the WM microstructure and WM injury severity in DOC patients have been published (Galanaud et al., 2012; Luyt et al., 2012). Laureys et al. (2006) reported increased fractional anisotropy (FA) in posteromedial cortical areas encompassing the cuneus and precuneus in a patient who remained in MCS for 19 years. Fernandez-Espejo et al. (2011) reported that patients with VS/UWS and MCS had significantly different mean diffusivity (MD) values in the subcortical WM and thalamus, but not in the brainstem. Lant et al. (2016) observed that DOC patients showed reduced FA in subcortico-cortical and cortico-cortical fiber tracts compared with controls.

The development of modern brain mapping techniques has enabled complex network analysis and description of the important properties of complex systems by quantifying topologies of their respective network representations. These methods aim to characterize brain networks with a small number of neurobiologically meaningful and easily computable measures (Rubinov and Sporns, 2010), which have been widely used to study patients with various forms of brain injury (Catani and Ffytche, 2005; Sporns, 2011), including patients with DOC (Demertzi et al., 2015; Wu et al., 2015). Crone et al. (2014) reported that compared with healthy subjects, the modularity, a graph theory property, is reduced in patients with VS/UWS and those in MCS; however, the path length and global efficiency did not differ between the groups. Pandit et al. (2013), who also used a graph theory approach, observed that the small-world topology was impaired in traumatic brain injury. Further work has shown that the global connectivity during rest is associated with the Coma Recovery Scale-Revised (CRS-R) total score and arousal subscale score (Amico et al., 2017). Recently, Weng et al. (2017) reported abnormal structural connectivity between the basal ganglia, thalamus, and frontal cortex in patients with DOC. They used a network-based statistical analysis and directly characterized the topological properties of brain axonal fiber profiles in DOC patients. However, no significant difference was found between the MCS and VS/UWS. However, few reports have examined alterations in the topological metrics of WM structural networks in patients with DOC.

The recent introduction of ultra-high-field MRI at 7 tesla (7 T) vastly improves the image signal-to-noise ratio relative to images obtained at lower field strengths. This approach also enables the acquisition of images with a high resolution and high contrast-to-noise ratio (van der Kolk et al., 2013). As such, it is a powerful means of non-invasively assessing normal and abnormal brain tissue with a high spatial resolution. In the current study, a simultaneous multi-slice (SMS) sequence (Moeller et al., 2010; Setsompop et al., 2012; Xu et al., 2013) of CMRR C2P for 7 T diffusion MRI (Vu et al., 2015; Sotiropoulos et al., 2016; Gulban et al., 2018) was used to acquire diffusion data in a shorter time. We aimed to analyze the network properties of brain WM profiles in DOC patients and track WM changes during the recovery process. The resultant data should provide a better understanding of DOC and aid in the early prediction of the recovery outcomes in patients with DOC.

2. Methods

2.1. Participants

Thirty patients with severe brain injuries and 11 healthy volunteers participated in the experiment. All the patients were from the Department of Rehabilitation in the Hangzhou Hospital of Zhejiang (CAPR), Hangzhou, China, from September 2016 to July 2018. Ethical approval was obtained from the Local Research Ethics Committee of the First Affiliated Hospital of Zhejiang University. Coma Recovery Scale-Revised (CRS-R) (Giacino et al., 2004) was used to estimate the patients' clinical condition on the 3 consecutive days before 7 T MRI scan by the same two medical doctors. The inclusion criteria for the patients were as follows: 1) disease course longer than 1 month but shorter than 1 year, 2) no history of psychological disorders, 3) no previous alcohol or drug abuse, 4) no epilepsy or frequent spontaneous movements, 5) no use of the benzodiazepine class of drugs, 6) no moderate or severe hydrocephalus (excluded with 1.5 T MRI data), and 7) no metal in any part of the body for security reasons. Eleven patients were excluded owing to MRI contraindications, and seven patients were excluded owing to the presence of extensive focal brain damage. One patient's data were excluded from the analysis due to a diagnosis of locked-in syndrome (see Table S1 for details). Finally, the data from 11 patients with severe brain injuries were included in the analysis. Additionally, 11 age- and sex-matched healthy control subjects were enrolled. None of the controls had a history of psychiatric or neurological illness, psychoactive drug consumption, or drug or alcohol abuse.

All procedures performed in this study were approved by the Ethics Committee of the First Affiliated Hospital, School of Medicine, Zhejiang University, and written informed consents in accordance with the Declaration of Helsinki were obtained from healthy participants and the legal guardians of the patients to allow them to participate in the study and for this article to be published.

2.2. Image acquisition

The MRI scan was performed with a 7 T research scanner (Siemens Healthcare, Erlangen, Germany) equipped with a Nova 1Tx/32Rx head coil (Nova Medical, Wilmington, MA, USA). Whole brain scanning was performed with sagittal T1-weighted magnetization-prepared rapid gradient echo (MPRAGE) 0.75 mm isotropic, 208 slices, echo time (TE)/repetition time (TR)/inversion time (TI) = 2.51/2590/1050 ms, flip angle (FA) = 7°, generalized autocalibrating partially parallel acquisitions (GRAPPA) = 2, acquisition time (TA) = 5′49″. The parameters employed for SMS DTI were: 1.25 mm isotropic, TE/TR = 66.2/5100 ms, FA = 90°, GRAPPA = 3, multi-band (MB) = 2, b = 2000 s/mm^2, 60 directions, TA = 6′53″, performed twice with opposite phase encoding directions with 112 slices for each direction. Six interspersed b0 images (non-diffusion weighted, b-value = 0 s/mm^2) were also acquired. High-dielectric pads (Zhao et al., 2018; Teeuwisse et al., 2012; Luo et al., 2013) were applied in one patient to enhance the signal in the brain regions.

2.3. Image preprocessing

Structural segmentation and normalization into Montreal Neurological Institute space (MNI-152) were performed by using the CONN functional connectivity toolbox (www.nitrc.org/projects/conn) (Whitfield-Gabrieli and Nieto-Castanon, 2012). Scans were inspected to ensure appropriate normalization (Fig. S2). All DTI data was preprocessed in FSL (Jenkinson et al., 2012) (http://fsl.fmrib.ox.ac.uk/fsl). Diffusion preprocessing for motion, susceptibility and eddy current distortion corrections were performed with FSL's eddy and topup tools (Andersson et al., 2003). To reduce the effect of excessive head motion during DTI acquisition, only participants who showed limited head movement during imaging acquisition (i.e., translation: < 3 mm;

rotation: < 2°; maximum absolute head motion: < 4 mm) were included in the study. In addition, all images were visually inspected to ensure the absence of artifacts. Non-brain regions were removed from the b0 images using the brain extraction tool (BET). Whole-brain images of diffusion metrics, including FA and MD were obtained via DTIFIT, which was used to calculate the diffusion tensor model at each voxel. The FA and MD were used to quantify the degree of WM disruption (Le Bihan et al., 2001).

2.4. Tract-based spatial statistics

Voxel-wise statistical analysis of the diffusion data, including the FA and MD images, between patients with DOC and healthy controls was performed using tract-based spatial statistics (TBSS) (Smith et al., 2006). All subjects' FA data were nonlinearly aligned to the predefined FSL FMRIB FA map and registered to the MNI-152 standard space. Next, a mean FA skeleton was created, which represented the centers of all tracts common to the group. The aligned FA and non-FA data of each participant was projected onto this skeleton. Two-sample nonparametric *t*-tests were used to obtain group differences between patients with DOC and healthy controls, with age and sex as covariates. The number of permutations was set at 5000. All resulting statistical maps were family wise error (FWE) corrected based on the threshold-free cluster enhancement (TFCE) option. The threshold for statistical significance was set at $p < .05$.

2.5. Node and edge definition

Diffusion post-processing and analysis were conducted using DSI Studio (http://dsi-studio.labsolver.org). A brain network can be described as a graph with nodes (brain regions) and edges that form connections between the nodes (Wen et al., 2017). The automated anatomic labelling (AAL) atlas including a total of 116 cortical and subcortical regions was used to define the nodes in this article. And each edge represented the number of streamlines interconnecting each pair of nodes.

2.6. Fiber tracking

We used a deterministic fiber-tracking algorithm (Yeh et al., 2013) as described in our previous study (Tan et al., 2018). Spin distribution functions were reconstructed in MNI space using q-space diffeomorphic reconstruction (QSDR), which provides a direct way to make comparisons between groups (Yeh and Tseng, 2011, 2013).

2.7. Connectome construction and graph theory analyses

The overall pattern of WM connections between each pair of brain nodes was computed using binary matrices. Nodes were defined as the 116 brain regions of the AAL atlas. This resulted in a 116 × 116 interregional connectivity matrix, with each element populated by the number of streamlines that served as a measure of connectivity strength. The connectivity matrices and graph theoretical analysis were conducted using the DSI Studio and network-based statistic (NBS) Connectome (Zalesky et al., 2010). The following global network metrics were investigated: network density, transitivity, clustering coefficient, network characteristic path length, small world-ness, global efficiency, local efficiency, and assortativity coefficient. Table S2 lists the definitions and descriptions of the network metrics used in this study.

2.8. Diffusion MRI connectometry

Group connectometry in DSI Studio was used to investigate the correlation between the WM structure and each of the six CRS-R subscale scores (with age, sex, and etiology included as covariates). A detailed description of the diffusion MRI connectometry was provided in the Supplementary materials.

2.9. Longitudinal study of brain connectome metrics

In this study, one VS/UWS patient was scanned 1.5 months after brain trauma. At 5 months after the trauma, the patient had progressed to MCS and was scanned for a second time. Another patient with cerebral ischemia and hypoxia was also scanned twice. The first scan was performed 3 months after brain injury when the patient was in MCS. The second scan was performed 11 months after brain injury when the patient was still in MCS. Besides, a 35-year-old healthy male subject was scanned twice on two different days with the same scan protocol to access the reproducibility. Within-subject comparisons were made of the data of the two scans to observe any longitudinal differences in brain connectivity networks.

2.10. Identification of disrupted WM connections

The NBS was used to identify subnetworks (clusters of nodes and edges) comprising connections with a reduced streamline count in patients with DOC. A detailed description of NBS has been reported previously (Zalesky et al., 2010). Briefly, a two-sample *t*-test at each connection was firstly performed to test for significant between-group differences in the value of the connectivity value. Following this, a primary component-forming threshold ($p < .01$, uncorrected) was applied to form a set of suprathreshold connections. Finally, the significance of each connected component was obtained with respect to an empirical estimate of the null distribution of maximal component sizes (50,000 permutations), with the component size measured as the number of edges it comprised.

2.11. Statistical analysis

All statistical analyses were performed using R (R Foundation for Statistical Computing, Vienna, Austria). Considering the sample size of this study was small and some of the data were non-normally distributed, Exact Two-Sample Fisher-Pitman Permutation Test was used to compare the data of the DOC and healthy control groups. Meanwhile, Approximative K-Sample Fisher-Pitman Permutation Test (seed = 456) was used for comparing the data of the three groups (healthy controls, MCS, and VS/UWS). The test level was set at $\alpha = 0.05$. Pairwise post-hoc analysis was subsequently employed where significant main group differences were observed. The corrected significance threshold was $p < .05$ with Bonferroni correction. For the connectome metrics that showed significant differences in both analyses, we plotted the receiver operating characteristic (ROC) curve to determine whether it could clearly distinguish DOC from healthy controls. The relationship between connectome metrics and CRS-R scores were assessed using Pearson's correlation coefficient.

For the NBS analysis, to determine the significance levels of altered connectivity networks, general linear models were used to examine the mean difference in connectivity strength of any connected components between groups. The statistical significance of each connected component was obtained with respect to an empirical estimate of the null distribution of maximal component sizes (50,000 permutations), with the component size measured as the number of edges it comprised. Significant subnetworks were initially determined at $p < .05$ and further tested at $p < .01$ (both thresholds were permutation corrected). We reported any components that were significant at a *p*-value of 0.01 after family-wise error (FWE) correction. And the BrainNet Viewer (Xia et al., 2013) was used to display the subnetworks.

Table 1
Details of the clinical characteristics and scores on the CRS-R for the 11 DOC patients used in this study.

Index	Patient	Gender/age (years)	Etiology	Duration (months)	CRS-R (sub-scores)
1	VS/UWS 1	M/23	TBI, L-basal ganglia	1.5	4 (0/0/2/0/0/2)
2	VS/UWS 2	M/72	TBI, R-frontal-temporo-parietal lobe	3	4 (0/0/1/1/0/2)
3	VS/UWS 3	M/68	TBI, diffuse axonal injury	3	7 (1/1/2/1/0/2)
4	VS/UWS 4	M/53	TBI, R-frontal lobe	1.5	4 (0/0/2/0/0/2)
5	VS/UWS 5	F/36	HIE, cardiopulmonary arrest	3	4 (1/0/1/0/0/2)
6	MCS 1	M/56	TBI, R-frontal lobe	7	11 (2/3/4/0/0/2)
7	MCS 2	M/53	HIE, carbon monoxide poisoning	3.5	10 (1/3/4/0/0/2)
8	MCS 3	M/50	HIE, subarachnoid hemorrhage	5	14 (2/3/3/2/1/3)
9	MCS 4	M/49	TBI, diffuse axonal injury	3	9 (1/3/3/0/0/2)
10	MCS 5	M/16	TBI, R-frontal & L-parietal lobe	1.5	8 (1/1/3/1/0/2)
11	MCS 6	M/68	HIE, cardiopulmonary arrest	8	8 (1/3/1/1/0/2)

Abbreviations: MCS, Minimally Conscious State; VS/UWS, Vegetative State/Unresponsive Wakefulness Syndrome; HIE, Hypoxic Ischemic Encephalopathy; TBI, Traumatic Brain Injury; CRS-R, Coma Recovery Scale-Revised. R, right; L, left. CRS-R sub-scores: auditory-visual-motor-oromotor-communication-arousal.

3. Results

3.1. Demographic information

Eleven patients with severe brain injuries were enrolled based on their CRS-R score and 1.5 T MRI scans. Five patients were diagnosed with VS, and six patients were diagnosed with MCS. Eleven age- and sex-matched healthy control subjects were also assessed. All patients and control subjects included in the study were right-handed. The clinical characteristics of the enrolled patients are shown in Table 1. All T1-weighted MPRAGE brain structural images for the 11 patients with DOC in this study are presented in Fig. S1 and representative axial, coronal, and sagittal images for patients from normalized structural dataset are shown with the overlying MNI template in Fig. S2. The demographic data of the two groups are shown in Table 2. There were no significant between-group differences for age or sex between patients and healthy controls ($p > .05$). Further, no significant group differences in head motion were observed.

3.2. Widespread WM disruption in patients with DOC

Fig. 1 shows the differences in FA and MD between patients with DOC and healthy controls, as identified through the voxel-wise TBSS analysis. Widespread FA reductions in the WM of patients with DOC were observed compared with the FA in healthy controls. Patients with DOC also exhibited higher MD in almost the entire WM skeleton relative to controls at the same contrast. Conversely, no WM regions with higher FA or lower MD in patients with DOC relative to controls were found.

Table 2
Demographic and clinical characteristics.

	DOC	HC	p-Value
Number	11	11	NA
Age/years, median (range)	52(16–72)	52(24–67)	NA
Sex, male (%)	90.91%	90.91%	NA
Handedness, right (%)	100%	100%	NA
Diagnosis (MCS/VS/UWS)	6/5	NA	NA
Etiology (HIE/TBI)	4/7	NA	NA
Translation of DTI scan (mm)	0.38 ± 0.17	0.47 ± 0.26	0.38[b]
Rotation of DTI scan (degree)	0.709 ± 0.368	0.575 ± 0.285	0.35[b]

Abbreviations: MCS, Minimally Conscious State; VS/UWS, Vegetative State/Unresponsive Wakefulness Syndrome; HIE, Hypoxic Ischemic Encephalopathy; TBI, Traumatic Brain Injury; CRS-R, Coma Recovery Scale-Revised. N/A, not applicable.

[b] *p*-Value was obtained using the two-sample two-tailed *t*-test.

3.3. Connectome metrics in patients with DOC compared to healthy controls

Significant between-group differences were detected for transitivity ($p < .001$), local efficiency ($p = .009$), and clustering coefficient ($p = .039$). All three metrics were significantly increased in DOC patients compared with healthy controls (Fig. 2).

3.4. Comparison of connectome metrics among healthy controls, MCS, and VS/UWS

Fig. 3 shows the connectome metrics of the healthy controls, MCS, and VS/UWS groups. Controlling for age and gender, statistical analysis showed significant group differences in transitivity ($p < .001$) and local efficiency ($p = .031$). Post-hoc analyses indicated that the VS group had greater transitivity compared with that of healthy controls ($p < .001$, Bonferroni corrected) and MCS ($p = .0217$, Bonferroni corrected). The VS group had greater local efficiency compared with that of healthy controls ($p = .039$, Bonferroni corrected). There was no significant difference between healthy controls and MCS for local efficiency after post-hoc analyses. There were no significant group differences in the remaining connectome metrics ($p > .05$).

3.5. ROC curve analysis

Fig. 4 shows the differentiation rate derived from ROC analysis for the brain connectome metrics of transitivity. With good classification accuracy, the value of transitivity that was significantly increased had the greatest ability to distinguish DOC patients from controls (AUC = 0.9871, sensitivity = 1.000, specificity = 1.000, efficiency = 1.000; $p < .001$).

3.6. Correlation between transitivity and CRS-R scores

As shown in Fig. 5, the value of transitivity showed a significant negative correlation with the CRS-R score, with a correlation coefficient of −0.6902 ($p < .05$).

3.7. Diffusion connectometry results

The connectometry analysis identified tracks with enhanced connectivity that were related to the CRS-R subscale score of language (false discovery rates = 0.09) in patients with DOC (Fig. S3). Widespread WM regions were correlated with the language subscale score. The relationships between the tract connectivity and other CRS-R subscale scores had high false discovery rates (> 0.50).

3.8. Longitudinal study of brain connectome metrics

Table 3 lists the detailed information of the two patients who

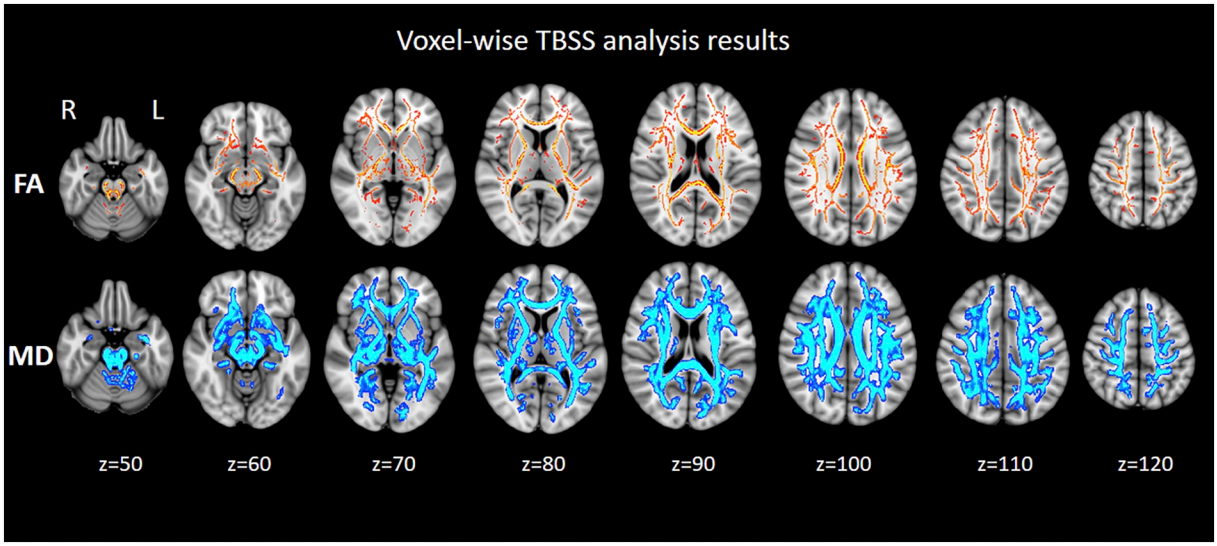

Fig. 1. Results of the voxel-wise tract-based spatial statistics (TBSS) analysis of the differences in fractional anisotropy (FA) and mean diffusivity (MD) between patients with DOC and healthy controls. Red-yellow represents areas with reduced FA, whereas blue-light represents areas with elevated MD in the DOC vs. healthy control group (thickened for better visibility).

participated in the longitudinal study. In addition, Fig. S3 displays the fractional anisotropy (FA) maps of patients' brain in the longitudinal study. (A) 1.5 months and (B) 5 months after initial injury for patient 01. (C) 3.5 months and (D) 11 months after initial injury for patient 07. Zoomed in coronal view of DTI principal direction of diffusion (PDD) maps overlaid on corresponding FA maps for patient 01 were shown in (E) 1.5 months and (F) 5 months after initial injury. Due to the high resolution, obvious white matter damage could be observed in the zoomed PDD maps for patient 01 in fig. S3(F). Fig. 6 shows that the value of transitivity for the patient who spontaneously recovered from UWS to MCS decreased in the second scan; however, the transitivity value was increased in the patient whose CRS-R score remained unchanged in the second scan. Furthermore, the intra-subject variation in transitivity for the healthy control participant was smaller than that for the patients.

3.9. Network-based statistical analysis of structural connectivity

Through NBS analysis and comparison between the DOC patients and healthy controls, a structural subnetwork was revealed, wherein the connectivity of this subnetwork was greater in the healthy controls than in the DOC patients. Specifically, this subnetwork of reduced connectivity in the DOC patients included 24 edges connecting 22 regions ($p = 6 * 10^{-5}$, FWE corrected). A significant difference was also observed in the strength of interhemispheric connection between the DOC group and the HC group.

All connections contributing to this subnetwork and their corresponding *t*-statistics are listed in Table 4. The nodes and edges contributing to this subnetwork are shown in Fig. 7, indicating that the subnetwork of decreased structural connectivity comprised of 22 nodes and is positioned in the frontal cortex, occipital lobe, and limbic system.

4. Discussion

This study investigated the whole-brain WM connectome in patients with DOC and healthy controls. The main findings yielded from the current study were as follows. First, DOC patients displayed elevated transitivity, local efficiency, and clustering coefficient of connectome metrics compared to those of healthy controls. When comparing the connectome metrics within the three groups (healthy controls, MCS, and VS/UWS), the VS group had greater transitivity compared with that of healthy controls and MCS. Notably, the connectivity alterations of transitivity significantly differentiated the diagnostic groups. Second, a longitudinal evaluation of brain connectome metrics in two patients showed that transitivity decreased in the patient who recovered from VS/UWS to MCS. In contrast, the patient whose CRS-R score remained unchanged demonstrated increased transitivity compared with the value obtained 10 months prior, which was consistent with its negative correlation with CRS-R score. Finally, NBS analysis revealed significantly decreased structural connectivity, which consisted of 22 nodes mainly in the frontal cortex, limbic system, occipital, and parietal lobes.

Consistent with prior findings, both the DOC patients and healthy controls in our study had small-world properties in their WM networks (Bullmore and Bassett, 2011; Crone et al., 2014; Weng et al., 2017). Small-world refers to networks that have similar characteristic path lengths but are more clustered, as opposed to random networks (Watts and Strogatz, 1998). Their topology reflects an optimal balance between global integration, which is essential for the high level functioning of human brain networks (Honey and Sporns, 2008). We observed that DOC patients showed increased small-world properties, which contrasts with the findings of Weng et al. (2017); however, this increase did not reach statistical significance. In our study, the DOC patients' networks showed significantly elevated clustering coefficient and local efficiency, although characteristic path length and global efficiency were similar to those of healthy controls. Elevated local efficiency, clustering coefficient, small-world properties, and similar characteristic path lengths in DOC patients may indicate more efficient use of local neural resources in DOC (Wen et al., 2017).

In the present study, the DOC patients' networks had greater transitivity, an outcome that has not been previously reported in the DOC graph theory literature. In our study, transitivity and clustering coefficient were both elevated in DOC patients compared with healthy controls. However, when comparing the metrics among healthy controls, MCS, and VS/UWS, only transitivity displayed significant differences among the three groups. Transitivity reflects the likelihood of a network to have interconnected nodes adjacent to one another and to be regulated by the global network. It is a more robust parameter than the clustering coefficient and is often used as an alternative to the latter, as it is not influenced by nodes with fewer connections (Newman, 2003). Our findings suggest that the distribution of information processing may be restricted to a group of densely interconnected regions

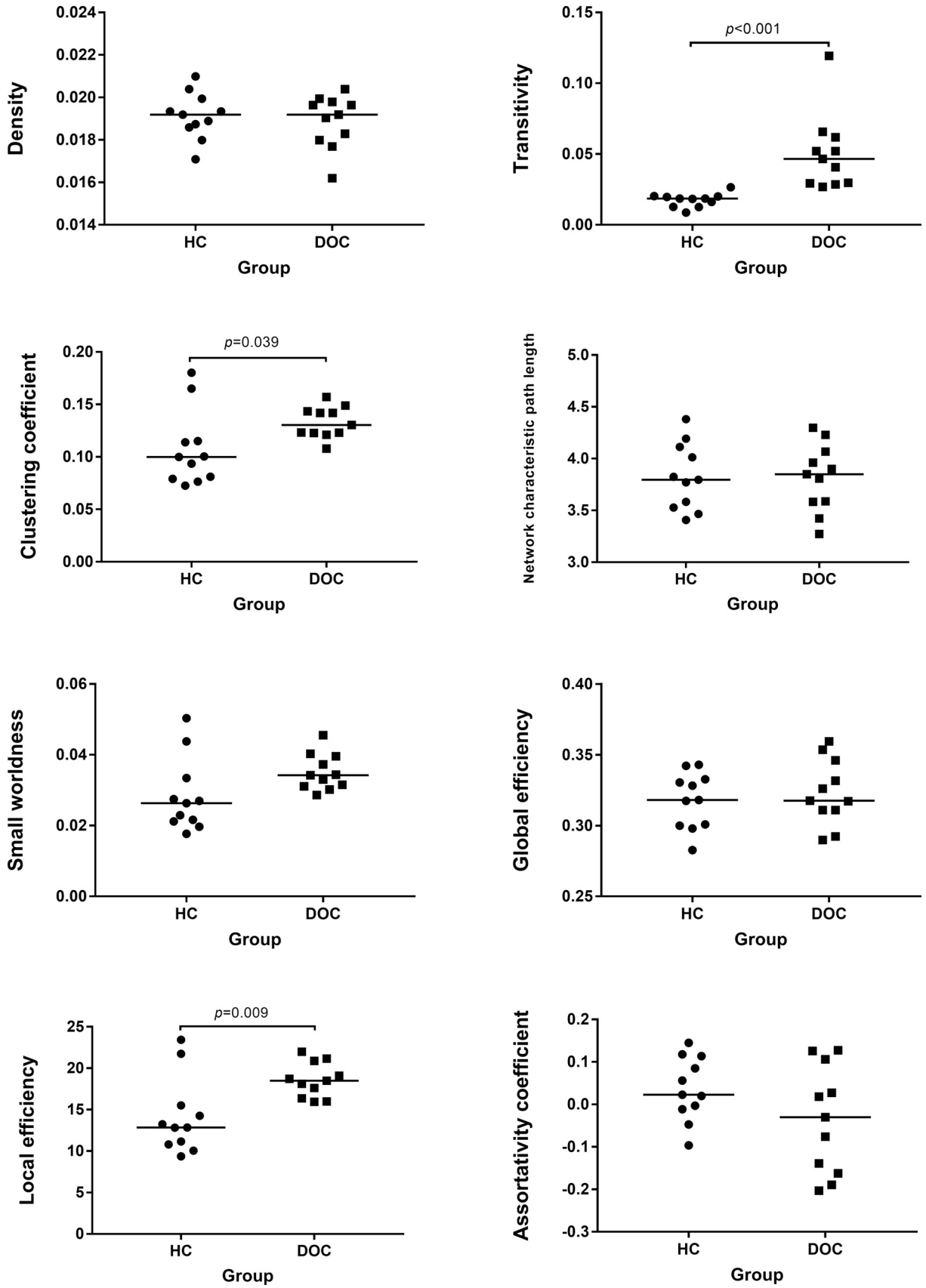

Fig. 2. Global topologic network parameters of brain white matter comparing disorders of consciousness (DOC) patients with healthy controls (HC). The horizontal scale represents the different groups, while the vertical scale refers to the values of connectome metrics. The short lines stand for their median for each group.

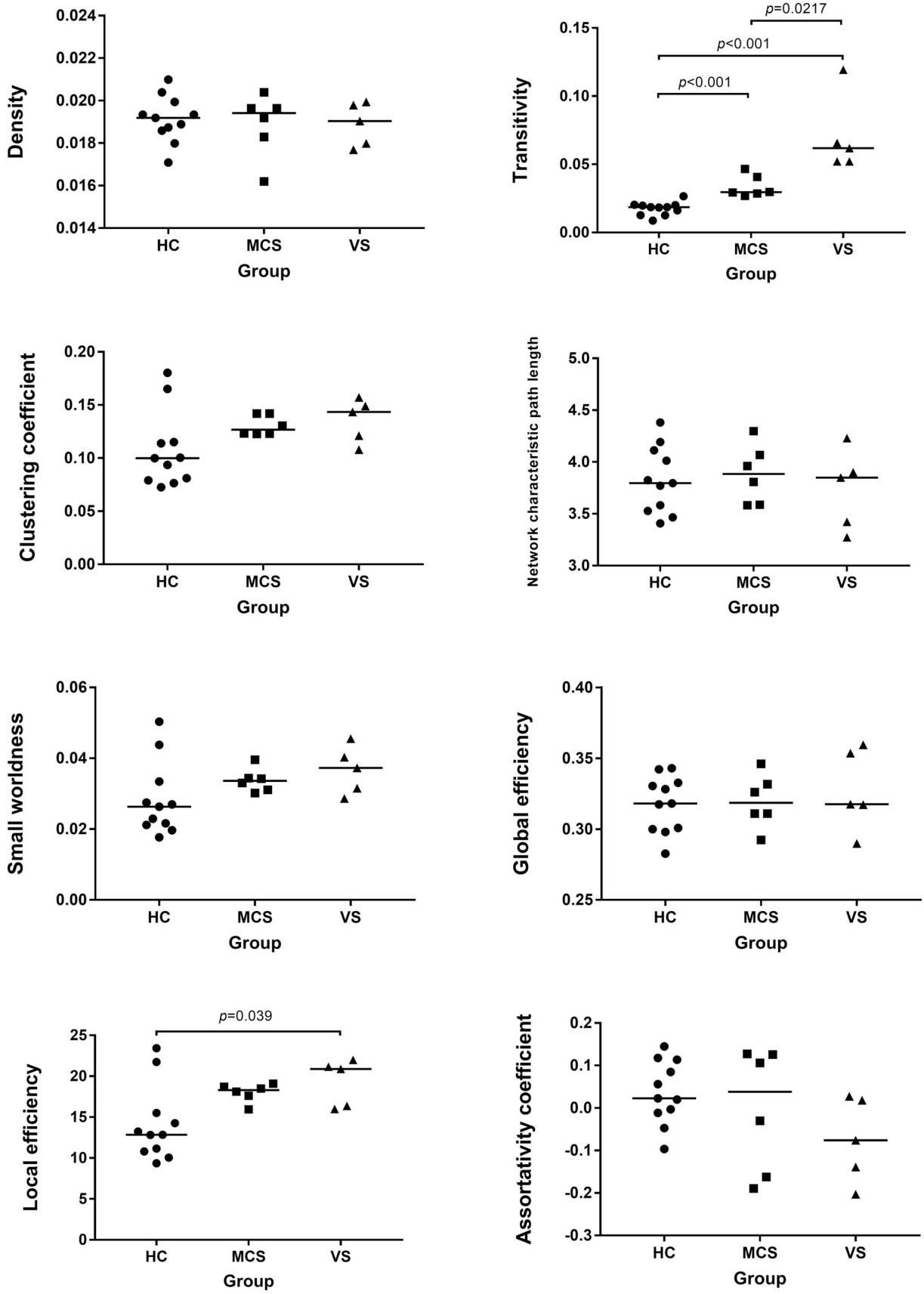

Fig. 3. Global topologic network parameters of brain white matter comparing among healthy controls (HC), minimally conscious state (MCS), and vegetative state/unresponsive wakefulness syndrome (VS/UWS). The horizontal scale represents the different groups, while the vertical scale refers to the values of connectome metrics. The short lines stand for their median for each group.

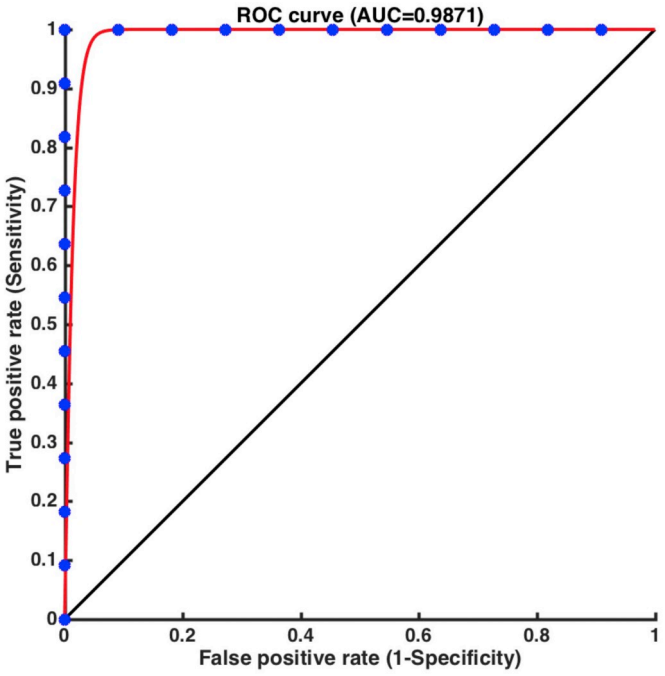

Fig. 4. ROC curve of transitivity based on structural connections. Transitivity had a strong ability to discriminate the disorders of consciousness (DOC) patients from healthy controls (AUC = 0.9871).

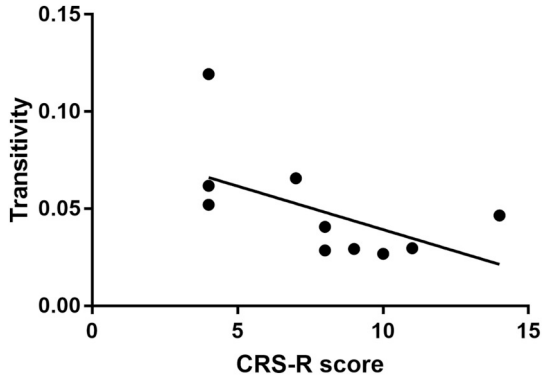

Fig. 5. Values of transitivity (y-axis) correlated to CRS-R scores (x-axis) with a correlation coefficient of −0.6902. CRS-R: Coma Recovery Scale-Revised.

of the brain network in DOC patients. A similar dichotomy of intergroup differences in clustering has previously emerged in graph theory studies of Alzheimer's disease (Daianu et al., 2015; de Haan et al., 2009) and late life depression (Ajilore et al., 2014; Li et al., 2015). More importantly, in this study, a significant difference in transitivity was found between the MCS and VS/UWS groups. A similar trend was observed in the two patients examined longitudinally, which is consistent

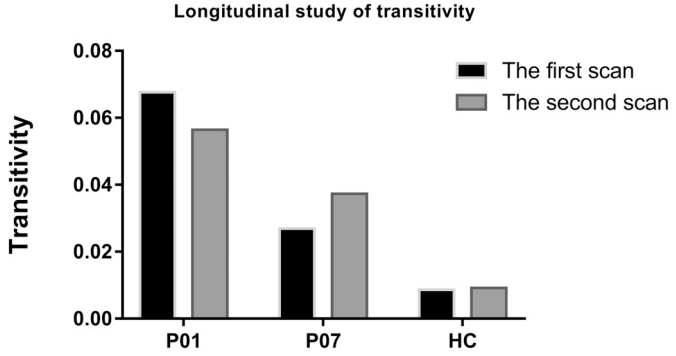

Fig. 6. Values of transitivity (y-axis) for subjects in the longitudinal study of brain connectome metrics.

with its negative correlation with CRS-R. It remains to be confirmed in further studies whether transitivity can be used as an auxiliary diagnostic tool to differentiate MCS from VS/UWS, or as an indicator for early prognosis of recovery outcomes in DOC patients.

A subnetwork that decreased structural connections was identified using the NBS approach. However, our results were discordant with those of Weng et al. (2017), who reported abnormal structural connectivity between the basal ganglia, thalamus, and frontal cortex in DOC patients. Our subnetwork consisted of 22 nodes among the frontal cortex, limbic system, occipital, and parietal lobes. Nine of 22 nodes were located in the frontal cortex. The frontal cortex constitutes two thirds of the human brain and plays an important role in a multitude of cognitive processes, such as executive function, attention, memory, and language (Chayer and Freedman, 2001). The medial prefrontal cortex (mPFC) participates in virtually all self-related processing: affecting human identity, altering attentional processes, decision-making, goal-directed behavior, and working memory (Goldman-Rakic et al., 1984; Vertes, 2004; Van Overwalle, 2009). Furthermore, the mPFC is a component of the DMN, which mediates internally oriented awareness and spontaneous cognition (Vanhaudenhuyse et al., 2011), and is widely reported in DOC (Crone et al., 2011; Kotchoubey et al., 2013; Vanhaudenhuyse et al., 2010; Norton et al., 2012). The mPFC is associated with consciousness level and its outcome in patients with acquired brain injury (Liu et al., 2017). Seven nodes were located in the limbic system. The cingulate cortex is also a component of the DMN. Chatelle et al. (2014) reported that the anterior cingulate cortex (ACC) could have an important role in pain processing and gating at the cortical level within the fronto-parietal network. Naro et al. (2015) used a repetitive transcranial magnetic stimulation (rTMS) approach to trigger fronto-parietal output in chronic DOC patients. They observed that rTMS over the ACC may be a useful approach to better investigate the level of consciousness impairment. Five nodes were located in the occipital lobe. Severe traumatic, anoxic, or hemorrhagic brain injuries can lead to VS/UWS in which the eyes are open but there is no evidence of a meaningful response; visual pursuit is considered to be one of the first signs appearing during recovery of consciousness (Giacino et al., 2002). The calcarine cortex is commonly defined as the primary visual

Table 3
Demographic and clinical characteristics of the DOC patients in the longitudinal study.

No.	Patient	Age (year)	Etiology	Time post-onset (months)	CRS-R	Total CRS-R score
P01	VS/UWS	23	TBI	1.5[a]/5[b]	0/0/2/0/0/2[a] 4/4/4/0/1/3[b]	4[a]/16[b]
P07	MCS	53	HIE	3.5[a]/11[b]	1/3/4/0/0/2[a] 1/3/4/0/0/2[b]	10[a]/10[b]

Abbreviations: MCS, Minimally Conscious State; VS/UWS, Vegetative State/Unresponsive Wakefulness Syndrome; HIE, Hypoxic Ischemic Encephalopathy; TBI, Traumatic Brain Injury; CRS-R, Coma Recovery Scale-Revised.

[a] The data from the first scan.

[b] The data from the second scan.

Table 4
Subnetwork composed of significantly decreased connections in the DOC patients compared to the healthy controls (HC), identified by a network-based statistic (NBS) approach ($p = 6.0 * 10^{-5}$, family-wise error (FWE) corrected).

Connection between	*t*-Stat	*p*-Value	Connection between	*t*-Stat	*p*-Value
Frontal_Sup_R-Supp_Motor_Area_L.	4.09	0.000569	Frontal_Sup_Medial_L-Occipital_Sup_L.	3.54	0.002067
Supp_Motor_Area_L-Supp_Motor_Area_R.	5.86	9.83E-06	Calcarine_R-Occipital_Sup_L.	3.18	0.004693
Frontal_Sup_L-Frontal_Sup_Medial_R.	3.29	0.003692	Cuneus_R-Occipital_Sup_L.	5.36	3.05E-05
Frontal_Mid_L-Frontal_Sup_Medial_R.	3.36	0.003099	Hippocampus_R-Precuneus_L.	3.29	0.003687
Supp_Motor_Area_L-Frontal_Sup_Medial_R.	3.71	0.00139	ParaHippocampal_L-Precuneus_L.	3.43	0.002625
Frontal_Sup_Medial_L-Frontal_Sup_Medial_R.	3.67	0.001535	Postcentral_R-Precuneus_L.	3.95	0.000791
Frontal_Sup_Medial_R-Cingulum_Ant_L.	3.16	0.004906	Supp_Motor_Area_R-Paracentral_Lobule_L.	4.85	9.75E-05
Supp_Motor_Area_L-Cingulum_Ant_R.	3.44	0.002561	Cingulum_Mid_R-Paracentral_Lobule_L.	3.41	0.002802
Frontal_Sup_Medial_L-Cingulum_Ant_R.	3.17	0.004798	Postcentral_R-Paracentral_Lobule_L.	3.16	0.004971
Supp_Motor_Area_L-Cingulum_Mid_R.	3.1	0.005615	Cingulum_Mid_L-Paracentral_Lobule_R.	3.75	0.001275
Calcarine_L-Cuneus_R.	3.37	0.003011	Precuneus_L-Paracentral_Lobule_R.	3.83	0.001051
Cuneus_L-Cuneus_R.	3.91	0.000867	Paracentral_Lobule_L-Paracentral_Lobule_R.	3.48	0.002343

L, left; R, right; table lists all connections that form part of the subnetwork identified as significant by NBS for comparison between DOC and HC arranged by the *t*-statistic for each connection.

cortex (Belliveau et al., 1991) or V1 (Lalli et al., 2006). An important role for visual sensory systems in early recovery of a patient who spontaneously recovered from VS/UWS to MCS with severe brain injury has been reported in our previous study (Tan et al., 2018). Finally, one node was located in the parietal lobe. Collectively, our subnetwork has been included in a meso-circuit model that attempts to explain DOC after brain injuries (Schiff, 2010). Although the thalamus was not in the subnetwork, the inclusion of the ACC is similarly recruited by a wide range of cognitive demands and shows graded activity with increasing cognitive load. This suggests that this component of the frontal executive systems may drive, or reciprocally increase activity, with the central thalamus in response to increasing cognitive demands (Stuss and Alexander, 2007).

There are several strengths to our study. First, ultra-high field (7 T) MRI was utilized to gain higher resolution, signal to noise ratio (SNR), and contrast-to-noise ratio (CNR). Vu et al. (2015) has reported that the higher spatial resolution of the 7 T data provides excellent detail including bands of low FA along the gray-white matter borders. Heidemann et al. (2012) also reported similar findings in zoomed dMRI studies with partial-brain coverage. In our study, obvious white matter damage could be observed in the zoomed PDD maps for patient 01 in the long longitudinal study due to the high resolution. Further analysis with the high resolution will be carried out in the future. Second, differences in network metrics for the structural connectome were observed not only between DOC patients and healthy controls, but also between MCS and VS/UWS. Furthermore, longitudinal examination of brain connectome metrics was performed, although only two patients were studied. Finally, a significant subnetwork was identified when comparing DOC patients with healthy controls, which may help to promote understanding of the mechanisms underlying DOC.

Several potential limitations of this study should be considered. First, the sample size was relatively small. As no metal in any body part was permitted in patients with DOC undergoing 7 T MRI scans, very few patients met the inclusion criteria. A second limiting factor was concern from family members. Third, the normalization of MR images was an issue in patients with DOC. Often, misalignment between the b0 images

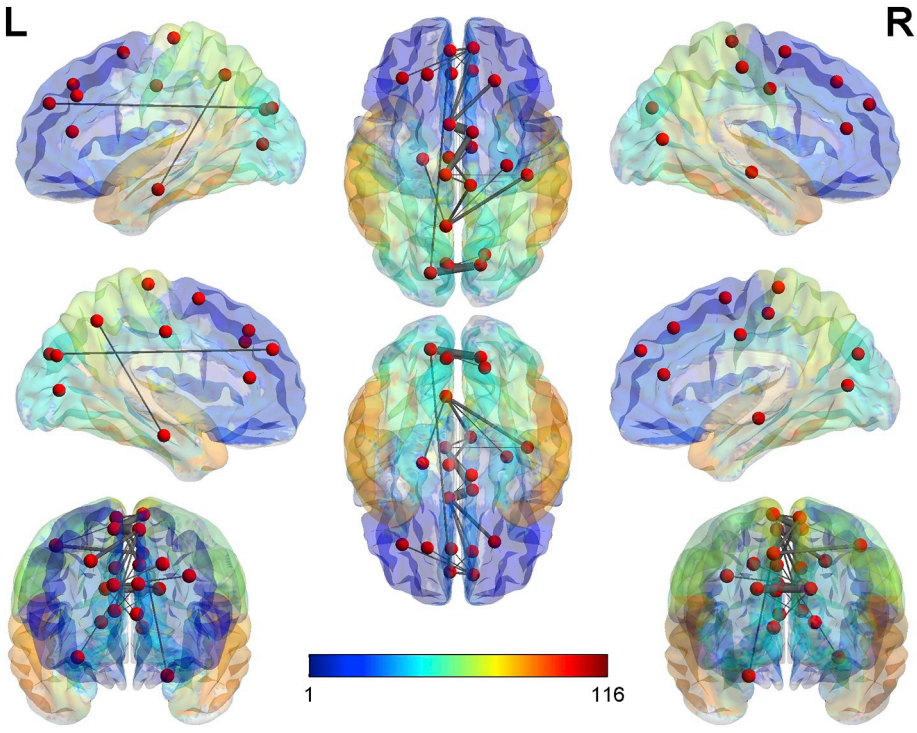

Fig. 7. The lateral and medial sides of each hemisphere, and the dorsal and ventral sides and the anterior and posterior sides of the subnetwork are shown. The nodes showing significant group differences comparing DOC patients with healthy controls are extracted from the AAL atlas and the radius of the edges represent the connectivity strengths between each pair of two nodes. Decreased structural connectivity, which consisted of 22 nodes mainly in the frontal cortex, limbic system, occipital, and parietal lobes.

and diffusion-weighted images for small ROIs can lead to imperfect registration to the MNI-152 space. Thus, we excluded patients with extensive focal brain damage. Fourth, considering the clinical feasibility and compliance, we did not perform 3 T MRI scanning for these patients, which resulted in the inability to perform comparisons among different field strengths (3 T and 7 T). In addition, more individualized analyses that take advantage of the 7 T resolution should be taken into consideration in the future. Finally, in this study, some of the patients with DOC had traumatic brain injury while others had hypoxic-ischemic encephalopathy, and as such, they had different pathogeneses. It would be better to divide patients into different subgroups based on the patients' various etiologies and to study the relationship between brain dysfunction and abnormal structural topologies in these different subgroups separately in the future.

5. Conclusions

In this study, non-invasive ultra-high field (7 T) MRI and graph theoretical analyses were used to reveal global network disruptions in DOC. The DOC network was highly segregated with significantly higher transitivity, local efficiency, and clustering coefficient of WM structural networks. Elevated transitivity in VS/UWS was also found compared with MCS. The findings from our longitudinal assessment also supported the view that transitivity would decrease if the patient's condition improved, which was consistent with its negative correlation with CRS-R score. A significant subnetwork was identified when comparing DOC patients with healthy controls, which may help to promote understanding of the mechanisms underpinning DOC. This preliminary study sheds light on the pivotal role of transitivity in distinguishing the various states of DOC based on graph theoretical approaches, which will help promote the cyborg intelligent systems (Wu et al., 2013, Yu et al., 2016) in the future.

Conflict of interest statement

None of the authors have potential conflicts of interest to be disclosed.

Author contributions

XT, GP, and BL were responsible for the study design, literature search, and manuscript drafting. XT, ZZ, JG, and FM were responsible for data collection and statistical analysis. YY, JZ, JW, FH, RW, and PGP were mainly responsible for administrative, technical, or material support. XZ, GP, and BL were responsible for the study concept and critical revision. All the authors contributed to editing of the manuscript.

Funding

This work was supported by the General Program of the National Natural Science Foundation of China (81870817), the Technology Project co-founded by Zhejiang Province and the Ministry of Health of China (2016152769), the National Key Research and Development Program of China (2016YFC1306402), Zhejiang Provincial Natural Science Foundation of China (LR15F020001), the Science and Technology Program of Zhejiang Province (2017C03011).

Acknowledgements

The authors would like to thank Doctor Sangma Xie in Hangzhou Dianzi University for assistance with optimizing scan parameters. The authors also express appreciation to Professor Chaozhe Zhu in State Key Laboratory of Cognitive Neuroscience and Learning, Beijing Normal University for valuable advice, Hongjian He and Bin Xu in Qiushi Academy for Advanced Studies, Zhejiang University for valuable support. In addition, Xufei Tan especially wishes to thank the teachers of ZiJing kindergarten in Sincere Garden, Hangzhou, China, for taking good care of her daughter when she prepared for this article.

Appendix A. Supplementary data

Supplementary data to this article can be found online at https://doi.org/10.1016/j.nicl.2019.101702.

References

Ajilore, O., Lamar, M., Leow, A., Zhang, A., Yang, S., Kumar, A., 2014. Graph theory analysis of cortical-subcortical networks in late-life depression. Am. J. Geriatr. Psychiatry 22, 195–206. https://doi.org/10.1016/j.jagp.2013.03.005.

Amico, E., Marinazzo, D., Di Perri, C., Heine, L., Annen, J., Martial, C., Dzemidzic, M., Kirsch, M., Bonhomme, V., Laureys, S., Goni, J., 2017. Mapping the functional connectome traits of levels of consciousness. NeuroImage 148, 201–211. https://doi.org/10.1016/j.neuroimage.2017.01.020.

Andersson, J.L., Skare, S., Ashburner, J., 2003. How to correct susceptibility distortions in spin-echo echo-planar images: application to diffusion tensor imaging. NeuroImage 20, 870–888. https://doi.org/10.1016/S1053-8119(03)00336-7.

Belliveau, J.W., Kennedy Jr., D.N., Mckinstry, R.C., Buchbinder, B.R., Weisskoff, R.M., Cohen, M.S., Vevea, J.M., Brady, T.J., Rosen, B.R., 1991. Functional mapping of the human visual cortex by magnetic resonance imaging. Science 254, 716–719.

Bodien, Y.G., Chatelle, C., Edlow, B.L., 2017. Functional networks in disorders of consciousness. Semin. Neurol. 37, 485–502. https://doi.org/10.1055/s-0037-1607310.

Boly, M., Tshibanda, L., Vanhaudenhuyse, A., Noirhomme, Q., Schnakers, C., Ledoux, D., Boveroux, P., Garweg, C., Lambermont, B., Phillips, C., Luxen, A., Moonen, G., Bassetti, C., Maquet, P., Laureys, S., 2009. Functional connectivity in the default network during resting state is preserved in a vegetative but not in a brain dead patient. Hum. Brain Mapp. 30, 2393–2400. https://doi.org/10.1002/hbm.20672.

Bullmore, E.T., Bassett, D.S., 2011. Brain graphs: graphical models of the human brain connectome. Annu. Rev. Clin. Psychol. 7, 113–140. https://doi.org/10.1146/annurev-clinpsy-040510-143934.

Catani, M., Ffytche, D.H., 2005. The rises and falls of disconnection syndromes. Brain 128, 2224–2239. https://doi.org/10.1093/brain/awh622.

Chatelle, C., Thibaut, A., Whyte, J., De Val, M.D., Laureys, S., Schnakers, C., 2014. Pain issues in disorders of consciousness. Brain Inj. 28, 1202–1208. https://doi.org/10.3109/02699052.2014.920518.

Chayer, C., Freedman, M., 2001. Frontal lobe functions. Curr. Neurol. Neurosci. Rep. 1, 547–552.

Cremers, L.G., De Groot, M., Hofman, A., Krestin, G.P., Van Der Lugt, A., Niessen, W.J., Vernooij, M.W., Ikram, M.A., 2016. Altered tract-specific white matter microstructure is related to poorer cognitive performance: the Rotterdam Study. Neurobiol. Aging 39, 108–117. https://doi.org/10.1016/j.neurobiolaging.2015.11.021.

Crone, J.S., Ladurner, G., Holler, Y., Golaszewski, S., Trinka, E., Kronbichler, M., 2011. Deactivation of the default mode network as a marker of impaired consciousness: an fMRI study. PLoS One 6, e26373. https://doi.org/10.1371/journal.pone.0026373.

Crone, J.S., Soddu, A., Holler, Y., Vanhaudenhuyse, A., Schurz, M., Bergmann, J., Schmid, E., Trinka, E., Laureys, S., Kronbichler, M., 2014. Altered network properties of the fronto-parietal network and the thalamus in impaired consciousness. Neuroimage Clin. 4, 240–248. https://doi.org/10.1016/j.nicl.2013.12.005.

Daianu, M., Jahanshad, N., Nir, T.M., Jack Jr., C.R., Weiner, M.W., Bernstein, M.A., Thompson, P.M., Alzheimer's Disease Neuroimaging, I., 2015. Rich club analysis in the Alzheimer's disease connectome reveals a relatively undisturbed structural core network. Hum. Brain Mapp. 36, 3087–3103. https://doi.org/10.1002/hbm.22830.

de Haan, W., Pijnenburg, Y.A., Strijers, R.L., Van Der Made, Y., Van Der Flier, W.M., Scheltens, P., Stam, C.J., 2009. Functional neural network analysis in frontotemporal dementia and Alzheimer's disease using EEG and graph theory. BMC Neurosci. 10, 101. https://doi.org/10.1186/1471-2202-10-101.

Demertzi, A., Antonopoulos, G., Heine, L., Voss, H.U., Crone, J.S., De Los Angeles, C., Bahri, M.A., Di Perri, C., Vanhaudenhuyse, A., Charland-Verville, V., Kronbichler, M., Trinka, E., Phillips, C., Gomez, F., Tshibanda, L., Soddu, A., Schiff, N.D., Whitfield-Gabrieli, S., Laureys, S., 2015. Intrinsic functional connectivity differentiates minimally conscious from unresponsive patients. Brain 138, 2619–2631. https://doi.org/10.1093/brain/awv169.

Fernandez-Espejo, D., Bekinschtein, T., Monti, M.M., Pickard, J.D., Junque, C., Coleman, M.R., Owen, A.M., 2011. Diffusion weighted imaging distinguishes the vegetative state from the minimally conscious state. NeuroImage 54, 103–112. https://doi.org/10.1016/j.neuroimage.2010.08.035.

Galanaud, D., Perlbarg, V., Gupta, R., Stevens, R.D., Sanchez, P., Tollard, E., De Champfleur, N.M., Dinkel, J., Faivre, S., Soto-Ares, G., Veber, B., Cottenceau, V., Masson, F., Tourdias, T., Andre, E., Audibert, G., Schmitt, E., Ibarrola, D., Dailler, F., Vanhaudenhuyse, A., Tshibanda, L., Payen, J.F., Le Bas, J.F., Krainik, A., Bruder, N., Girard, N., Laureys, S., Benali, H., Puybasset, L., Neuro Imaging for Coma, E., and Recovery, C, 2012. Assessment of white matter injury and outcome in severe brain trauma: a prospective multicenter cohort. Anesthesiology 117, 1300–1310. https://doi.org/10.1097/ALN.0b013e3182755558.

Giacino, J.T., Ashwal, S., Childs, N., Cranford, R., Jennett, B., Katz, D.I., Kelly, J.P., Rosenberg, J.H., Whyte, J., Zafonte, R.D., Zasler, N.D., 2002. The minimally conscious state: definition and diagnostic criteria. Neurology 58, 349–353.

Giacino, J.T., Kalmar, K., Whyte, J., 2004. The JFK Coma Recovery Scale-revised:

measurement characteristics and diagnostic utility. Arch. Phys. Med. Rehabil. 85, 2020–2029.
Goldman-Rakic, P.S., Selemon, L.D., Schwartz, M.L., 1984. Dual pathways connecting the dorsolateral prefrontal cortex with the hippocampal formation and parahippocampal cortex in the rhesus monkey. Neuroscience 12, 719–743.
Gulban, O.F., De Martino, F., Vu, A.T., Yacoub, E., Ugurbil, K., Lenglet, C., 2018. Cortical fibers orientation mapping using in-vivo whole brain 7T diffusion MRI. NeuroImage 178, 104–118. https://doi.org/10.1016/j.neuroimage.2018.05.010.
Heidemann, R.M., Anwander, A., Feiweier, T., Knosche, T.R., Turner, R., 2012. K-space and q-space: combining ultra-high spatial and angular resolution in diffusion imaging using ZOOPPA at 7T. NeuroImage 60, 967–978. 10.1016/j.neuroimage.2011.12.081.
Honey, C.J., Sporns, O., 2008. Dynamical consequences of lesions in cortical networks. Hum. Brain Mapp. 29, 802–809. https://doi.org/10.1002/hbm.20579.
Jenkinson, M., Beckmann, C.F., Behrens, T.E., Woolrich, M.W., Smith, S.M., 2012. Fsl. NeuroImage 62, 782–790. https://doi.org/10.1016/j.neuroimage.2011.09.015.
Kotchoubey, B., Merz, S., Lang, S., Markl, A., Muller, F., Yu, T., Schwarzbauer, C., 2013. Global functional connectivity reveals highly significant differences between the vegetative and the minimally conscious state. J. Neurol. 260, 975–983. https://doi.org/10.1007/s00415-012-6734-9.
Lalli, S., Hussain, Z., Ayub, A., Cracco, R.Q., Bodis-Wollner, I., Amassian, V.E., 2006. Role of the calcarine cortex (V1) in perception of visual cues for saccades. Clin. Neurophysiol. 117, 2030–2038. https://doi.org/10.1016/j.clinph.2006.05.022.
Lant, N.D., Gonzalez-Lara, L.E., Owen, A.M., Fernandez-Espejo, D., 2016. Relationship between the anterior forebrain mesocircuit and the default mode network in the structural bases of disorders of consciousness. Neuroimage Clin. 10, 27–35. https://doi.org/10.1016/j.nicl.2015.11.004.
Laureys, S., Boly, M., Maquet, P., 2006. Tracking the recovery of consciousness from coma. J. Clin. Invest. 116, 1823–1825. https://doi.org/10.1172/JCI29172.
Laureys, S., Celesia, G.G., Cohadon, F., Lavrijsen, J., Leon-Carrion, J., Sannita, W.G., Sazbon, L., Schmutzhard, E., Von Wild, K.R., Zeman, A., Dolce, G., European Task Force on Disorders Of, C, 2010. Unresponsive wakefulness syndrome: a new name for the vegetative state or apallic syndrome. BMC Med. 8, 68. https://doi.org/10.1186/1741-7015-8-68.
Le Bihan, D., Mangin, J.F., Poupon, C., Clark, C.A., Pappata, S., Molko, N., et al., 2001. Diffusion tensor imaging: concepts and applications. J MRI 13 (4), 534–546.
Li, W., Douglas Ward, B., Liu, X., Chen, G., Jones, J.L., Antuono, P.G., Li, S.J., Goveas, J.S., 2015. Disrupted small world topology and modular organisation of functional networks in late-life depression with and without amnestic mild cognitive impairment. J. Neurol. Neurosurg. Psychiatry 86, 1097–1105. https://doi.org/10.1136/jnnp-2014-309180.
Liu, X., Li, J., Gao, J., Zhou, Z., Meng, F., Pan, G., Luo, B., 2017. Association of medial prefrontal cortex connectivity with consciousness level and its outcome in patients with acquired brain injury. J. Clin. Neurosci. 42, 160–166. https://doi.org/10.1016/j.jocn.2017.04.015.
Long, J., Xie, Q., Ma, Q., Urbin, M.A., Liu, L., Weng, L., Huang, X., Yu, R., Li, Y., Huang, R., 2016. Distinct interactions between fronto-parietal and default mode networks in impaired consciousness. Sci. Rep. 6, 38866. https://doi.org/10.1038/srep38866.
Luo, W., Lanagan, M.T., Sica, C.T., Ryu, Y., Oh, S., Ketterman, M., Yang, Q.X., Collins, C.M., 2013. Permittivity and performance of dielectric pads with sintered ceramic beads in MRI: early experiments and simulations at 3 T. Magn. Reson. Med. 70 (1), 269–275. https://doi.org/10.1002/mrm.24433.
Luyt, C.E., Galanaud, D., Perlbarg, V., Vanhaudenhuyse, A., Stevens, R.D., Gupta, R., Besancenot, H., Krainik, A., Audibert, G., Combes, A., Chastre, J., Benali, H., Laureys, S., Puybasset, L., Neuro Imaging for Coma, E., and Recovery, C, 2012. Diffusion tensor imaging to predict long-term outcome after cardiac arrest: a bicentric pilot study. Anesthesiology 117, 1311–1321. https://doi.org/10.1097/ALN.0b013e318275148c.
Mayer, A.R., Mannell, M.V., Ling, J., Gasparovic, C., Yeo, R.A., 2011. Functional connectivity in mild traumatic brain injury. Hum. Brain Mapp. 32, 1825–1835. https://doi.org/10.1002/hbm.21151.
Moeller, S., Yacoub, E., Olman, C.A., Auerbach, E., Strupp, J., Harel, N., Ugurbil, K., 2010. Multiband multislice GE-EPI at 7 tesla, with 16-fold acceleration using partial parallel imaging with application to high spatial and temporal whole-brain fMRI. Magn. Reson. Med. 63, 1144–1153. https://doi.org/10.1002/mrm.22361.
Naro, A., Russo, M., Leo, A., Bramanti, P., Quartarone, A., Calabro, R.S., 2015. A single session of repetitive transcranial magnetic stimulation over the dorsolateral prefrontal cortex in patients with unresponsive wakefulness syndrome: preliminary results. Neurorehabil. Neural Repair 29, 603–613. https://doi.org/10.1177/1545968314562114.
Nazeri, A., Chakravarty, M.M., Rajji, T.K., Felsky, D., Rotenberg, D.J., Mason, M., Xu, L.N., Lobaugh, N.J., Mulsant, B.H., Voineskos, A.N., 2015. Superficial white matter as a novel substrate of age-related cognitive decline. Neurobiol. Aging 36, 2094–2106. https://doi.org/10.1016/j.neurobiolaging.2015.02.022.
Newman, M.E.J., 2003. The structure and function of complex networks. SIAM Rev. 45, 167–256.
Norton, L., Hutchison, R.M., Young, G.B., Lee, D.H., Sharpe, M.D., Mirsattari, S.M., 2012. Disruptions of functional connectivity in the default mode network of comatose patients. Neurology 78, 175–181. https://doi.org/10.1212/WNL.0b013e31823fcd61.
Pandit, A.S., Expert, P., Lambiotte, R., Bonnelle, V., Leech, R., Turkheimer, F.E., Sharp, D.J., 2013. Traumatic brain injury impairs small-world topology. Neurology 80, 1826–1833. https://doi.org/10.1212/WNL.0b013e3182929f38.
Rubinov, M., Sporns, O., 2010. Complex network measures of brain connectivity: uses and interpretations. Neuroimage 52 (3), 1059–1069. 10.1016/j.neuroimage.2009.10.003.
Schiff, N.D., 2010. Recovery of consciousness after brain injury: a mesocircuit hypothesis. Trends Neurosci. 33, 1–9. https://doi.org/10.1016/j.tins.2009.11.002.
Setsompop, K., Gagoski, B.A., Polimeni, J.R., Witzel, T., Wedeen, V.J., Wald, L.L., 2012. Blipped-controlled aliasing in parallel imaging for simultaneous multislice echo planar imaging with reduced g-factor penalty. Magn. Reson. Med. 67, 1210–1224. https://doi.org/10.1002/mrm.23097.
Sharp, D.J., Scott, G., Leech, R., 2014. Network dysfunction after traumatic brain injury. Nat. Rev. Neurol. 10, 156–166. https://doi.org/10.1038/nrneurol.2014.15.
Shumskaya, E., Andriessen, T.M., Norris, D.G., Vos, P.E., 2012. Abnormal whole-brain functional networks in homogeneous acute mild traumatic brain injury. Neurology 79, 175–182. https://doi.org/10.1212/WNL.0b013e31825f04fb.
Smith, S.M., Jenkinson, M., Johansen-Berg, H., Rueckert, D., Nichols, T.E., Mackay, C.E., Watkins, K.E., Ciccarelli, O., Cader, M.Z., Matthews, P.M., Behrens, T.E., 2006. Tract-based spatial statistics: voxelwise analysis of multi-subject diffusion data. NeuroImage 31, 1487–1505. https://doi.org/10.1016/j.neuroimage.2006.02.024.
Smith, S.M., Fox, P.T., Miller, K.L., Glahn, D.C., Fox, P.M., Mackay, C.E., Filippini, N., Watkins, K.E., Toro, R., Laird, A.R., Beckmann, C.F., 2009. Correspondence of the brain's functional architecture during activation and rest. Proc. Natl. Acad. Sci. U. S. A. 106, 13040–13045. https://doi.org/10.1073/pnas.0905267106.
Sotiropoulos, S.N., Hernandez-Fernandez, M., Vu, A.T., Andersson, J.L., Moeller, S., Yacoub, E., Lenglet, C., Ugurbil, K., Behrens, T.E.J., Jbabdi, S., 2016. Fusion in diffusion MRI for improved fibre orientation estimation: an application to the 3 T and 7 T data of the Human Connectome Project. NeuroImage 134, 396–409. https://doi.org/10.1016/j.neuroimage.2016.04.014.
Sporns, O., 2011. The human connectome: a complex network. Ann. N. Y. Acad. Sci. 1224, 109–125. https://doi.org/10.1111/j.1749-6632.2010.05888.x.
Stuss, D.T., Alexander, M.P., 2007. Is there a dysexecutive syndrome? Philos. Trans. R. Soc. Lond. Ser. B Biol. Sci. 362, 901–915. https://doi.org/10.1098/rstb.2007.2096.
Tan, X.F., Gao, J., Zhou, Z., Wei, R.L., Gong, T., Wu, Y.Q., Liu, K.H., He, F.P., Wang, J.Y., Li, J.Q., Zhang, X.T., Pan, G., Luo, B.Y., 2018. Spontaneous recovery from unresponsive wakefulness syndrome to a minimally conscious state: early structural changes revealed by 7-T magnetic resonance imaging. Front. Neurol. 8, 741. https://doi.org/10.3389/fneur.2017.00741.
Teeuwisse, M., Brink, M., Webb, G., 2012. Quantitative assessment of the effects of high-permittivity pads in 7 Tesla MRI of the brain. Magn. Reson. Med. 67 (5), 1285–1293. https://doi.org/10.1002/mrm.23108.
Van Der Kolk, A.G., Hendrikse, J., Zwanenburg, J.J., Visser, F., Luijten, P.R., 2013. Clinical applications of 7 T MRI in the brain. Eur. J. Radiol. 82, 708–718. https://doi.org/10.1016/j.ejrad.2011.07.007.
Van Overwalle, F., 2009. Social cognition and the brain: a meta-analysis. Hum. Brain Mapp. 30, 829–858. https://doi.org/10.1002/hbm.20547.
Vanhaudenhuyse, A., Noirhomme, Q., Tshibanda, L.J., Bruno, M.A., Boveroux, P., Schnakers, C., Soddu, A., Perlbarg, V., Ledoux, D., Brichant, J.F., Moonen, G., Maquet, P., Greicius, M.D., Laureys, S., Boly, M., 2010. Default network connectivity reflects the level of consciousness in non-communicative brain-damaged patients. Brain 133, 161–171. https://doi.org/10.1093/brain/awp313.
Vanhaudenhuyse, A., Demertzi, A., Schabus, M., Noirhomme, Q., Bredart, S., Boly, M., Phillips, C., Soddu, A., Luxen, A., Moonen, G., Laureys, S., 2011. Two distinct neuronal networks mediate the awareness of environment and of self. J. Cogn. Neurosci. 23, 570–578. https://doi.org/10.1162/jocn.2010.21488.
Vertes, R.P., 2004. Memory consolidation in sleep; dream or reality. Neuron 44, 135–148. https://doi.org/10.1016/j.neuron.2004.08.034.
Vu, A.T., Auerbach, E., Lenglet, C., Moeller, S., Sotiropoulos, S.N., Jbabdi, S., Andersson, J., Yacoub, E., Ugurbil, K., 2015. High resolution whole brain diffusion imaging at 7 T for the Human Connectome Project. NeuroImage 122, 318–331. https://doi.org/10.1016/j.neuroimage.2015.08.004.
Watts, D.J., Strogatz, S.H., 1998. Collective dynamics of 'small-world' networks. Nature 393, 440–442. https://doi.org/10.1038/30918.
Wen, M.C., Heng, H.S.E., Hsu, J.L., Xu, Z., Liew, G.M., Au, W.L., Chan, L.L., Tan, L.C.S., Tan, E.K., 2017. Structural connectome alterations in prodromal and de novo Parkinson's disease patients. Parkinsonism Relat. Disord. 45, 21–27. https://doi.org/10.1016/j.parkreldis.2017.09.019.
Weng, L., Xie, Q., Zhao, L., Zhang, R., Ma, Q., Wang, J., Jiang, W., He, Y., Chen, Y., Li, C., Ni, X., Xu, Q., Yu, R., Huang, R., 2017. Abnormal structural connectivity between the basal ganglia, thalamus, and frontal cortex in patients with disorders of consciousness. Cortex 90, 71–87. https://doi.org/10.1016/j.cortex.2017.02.011.
Whitfield-Gabrieli, S., Nieto-Castanon, A., 2012. Conn: a functional connectivity toolbox for correlated and anticorrelated brain networks. Brain Connect. 2 (3), 125–141. https://doi.org/10.1089/brain.2012.0073.
Wu, Z.H., Pan, G., Zheng, N.G., 2013. Cyborg Intelligence. IEEE Intelligent Systems 28 (5), 31–33.
Wu, X., Zou, Q., Hu, J., Tang, W., Mao, Y., Gao, L., Zhu, J., Jin, Y., Wu, X., Lu, L., Zhang, Y., Zhang, Y., Dai, Z., Gao, J.H., Weng, X., Zhou, L., Northoff, G., Giacino, J.T., He, Y., Yang, Y., 2015. Intrinsic functional connectivity patterns predict consciousness level and recovery outcome in acquired brain injury. J. Neurosci. 35, 12932–12946. https://doi.org/10.1523/JNEUROSCI.0415-15.2015.
Xia, M., Wang, J., He, Y., 2013. BrainNet Viewer: a network visualization tool for human brain connectomics. PLoS One 8, e68910. https://doi.org/10.1371/journal.pone.0068910.
Xu, J., Moeller, S., Auerbach, E.J., Strupp, J., Smith, S.M., Feinberg, D.A., Yacoub, E., Ugurbil, K., 2013. Evaluation of slice accelerations using multiband echo planar imaging at 3 T. NeuroImage 83, 991–1001. https://doi.org/10.1016/j.neuroimage.2013.07.055.
Yeh, F.C., Tseng, W.Y., 2011. NTU-90: a high angular resolution brain atlas constructed by q-space diffeomorphic reconstruction. NeuroImage 58, 91–99. https://doi.org/10.1016/j.neuroimage.2011.06.021.
Yeh, F.C., Tseng, W.Y., 2013. Sparse solution of fiber orientation distribution function by diffusion decomposition. PLoS One 8, e75747. https://doi.org/10.1371/journal.

pone.0075747.
Yeh, F.C., Verstynen, T.D., Wang, Y., Fernandez-Miranda, J.C., Tseng, W.Y., 2013. Deterministic diffusion fiber tracking improved by quantitative anisotropy. PLoS One 8, e80713. https://doi.org/10.1371/journal.pone.0080713.
Yu, Y.P., Pan, G., Gong, Y.Y., Xu, K.D., Zheng, N., Hua, W.D., Zheng, X.X., Wu, Z.H., 2016. Intelligence-augmented rat cyborgs in maze solving. PLOS ONE 11 (2).
Zalesky, A., Fornito, A., Bullmore, E.T., 2010. Network-based statistic: identifying differences in brain networks. NeuroImage 53, 1197–1207. https://doi.org/10.1016/j.neuroimage.2010.06.041.
Zhao, J., Luo, W., Qian, M.Z., Sun, Y., Xia, L., Zhang, X.T., 2018. Evaluation of high-dielectric pads for macaque brain imaging at 7 T: a pilot study. Proc. Int. Soc. Mag. Reson Med. 26, 4302.
Zhou, Z., Wang, J.B., Zang, Y.F., Pan, G., 2018. PAIR comparison between two within-group conditions of resting-state fMRI improves classification accuracy. Front. Neurosci. 11, 740. https://doi.org/10.3389/fnins.2017.00740.